

## Article

# A Novel Measurement-Based Method for Assessing Global Warming Mitigation via High-Albedo Solutions

Federico Rossi <sup>1</sup>, Mirko Filipponi <sup>1,\*</sup>, Beatrice Castellani <sup>1</sup>, Stefania Bonafoni <sup>1</sup> and Chaouki Ghenai <sup>2</sup><sup>1</sup> Department of Engineering, University of Perugia, 06125 Perugia, Italy<sup>2</sup> Sustainable and Renewable Energy Engineering Department, University of Sharjah, Sharjah P.O. Box 27272, United Arab Emirates

\* Correspondence: mirko.filipponi@unipg.it; Tel.: +39-0744-492969

**Abstract:** Global warming mitigation via terrestrial albedo increase has been widely investigated in literature; the proposed methodologies relate CO<sub>2</sub> compensation to albedo increase generally via the concept of Radiative Forcing (RF). However, literature methods calculate RF by averaged input data, without considering RF variation due to many local and temporal phenomena. For instance, an average value of compensated effect of albedo change ( $\Delta\alpha = 0.01$ ) is 3 kg CO<sub>2eq</sub>/m<sup>2</sup>, which has been introduced no matter the position and climatic condition of the site. In our study, we propose a novel procedure to measure RF continuous time history by means of ground measurements, astronomical equations, and satellite calibration. The procedure is called RF-meter. In this way, a more accurate assessment of compensated CO<sub>2</sub> may be achieved. A test facility is also designed and proposed to double check the procedure, and preliminary results are reported in order to show and test the calibration procedure. It is expected that albedo-increased surfaces as well as cool roofs and/or other technical solutions will be eligible to obtain Emission Credits (EC). The proposed procedure will aid in the assignment of EC to High-Albedo Solutions (HAS), as it could represent an objective and accurate method to relate the albedo increase to a corresponding CO<sub>2</sub> offset.

**Keywords:** albedo; global warming; radiative forcing meter; emission credit

**Citation:** Rossi, F.; Filipponi, M.; Castellani, B.; Bonafoni, S.; Ghenai, C. A Novel Measurement-Based Method for Assessing Global Warming Mitigation via High-Albedo Solutions. *Energies* **2022**, *15*, 5695. <https://doi.org/10.3390/en15155695>

Academic Editor: Attilio Converti

Received: 11 July 2022

Accepted: 2 August 2022

Published: 5 August 2022

**Publisher's Note:** MDPI stays neutral with regard to jurisdictional claims in published maps and institutional affiliations.



**Copyright:** © 2022 by the authors. Licensee MDPI, Basel, Switzerland. This article is an open access article distributed under the terms and conditions of the Creative Commons Attribution (CC BY) license (<https://creativecommons.org/licenses/by/4.0/>).

## 1. Introduction

The IPCC (International Panel on Climatic Change) 5th Report [1] proposes several policies for mitigation and adaptation to climatic changes. Such policies must be translated into rules and laws by countries. Mitigation of global warming (GW) is generally achieved through the following major principles aimed to reduce the introduction of Greenhouse Gases (GHG) into Earth's atmosphere: the production of energy by renewables, energy efficiency, and Carbon Capture and Sequestration (CCS).

Programmatic initiatives are also introduced; the European Union (EU) and other national and transnational authorities have issued different ETSs (Emission Trading Schemes), i.e., a sort of stock exchange market of carbon [2]. The exchange unit, called emission credit, is 1 ton of CO<sub>2</sub>. On EU-ETS, the actual value attributed to 1 ton of CO<sub>2</sub> is around 100 €.

The only way to produce emission credits is by pursuing the above three major principles. However, the IPCC itself acknowledges that further principles may tackle global warming in addition to the increase of terrestrial albedo (IPCC 6th Assessment Report *RF* synoptic) [3].

Terrestrial albedo can be increased artificially via cool roofs [4], land-use modification, particular arboreal cultivation, and so on; we will call these High-Albedo Solutions (HAS).

As reported in Section 2, many authors and research groups have dealt with the direct relation of HAS and global warming mitigation. In literature, the concept of CO<sub>2</sub> compensation has been introduced; HAS produces a reduction on global temperature which is the same as if a corresponding amount of CO<sub>2</sub> would be taken off from the

atmosphere. The mentioned literature surveys, including the present authors' [5], are based on different models and calculus but all refer to the IPCC radiative forcing concept to determine the relation between HAS and CO<sub>2</sub>. Radiative forcing will be better discussed in Sections 2 and 3.

However, changes in radiative forcing produced by HAS take into account many factors that the literatures approaches do not involve. One is the continuous variation of the atmospheric absorption both on downward and upward energy paths because of weather air mass particle and aerosol also in addition to the albedo change because of weathering, dusting, fouling, and surface deterioration and the instantaneous solar energy change mainly because of the seasonal and daily solar path.

It is also important to highlight that cool roofs or HAS on built environments produce further indirect contributions to tackle global warming such as building energy savings, especially for Cooling Dominant Zone (CDZ) and Urban Heat Island (UHI) mitigation. However, such topics are widely investigated in the literature [6,7].

Finally, the calculus of CO<sub>2</sub> compensation requires an energy evaluation by the knowledge of the time history of radiative forcing. The present paper proposes a novel approach to better estimate the amount of CO<sub>2</sub> compensated by HAS; the approach is based on ground measurements which allow the determination of the radiative forcing time history. Moreover, a calibration procedure by satellite occasional measurements attributes a higher reliability to the proposed procedure. In this way, a particular HAS will be precisely characterized in terms of CO<sub>2</sub> offset evaluating also the time performances of compensation. The CO<sub>2</sub> compensation is correlated to the reduction of the radiative forcing through the conversion factors defined by the IPCC. The validation of the presented approach is based on the IPCC conversion factors and the data acquired from the test facility, installed on the roof of University of Perugia, in Perugia, Italy. An example of calibration, based on preliminary data, is also reported. It is hoped that the proposed methodology will facilitate the introduction of HAS into ETS as well as renewables, efficiency, and CCS.

## 2. Methods Review

In this section, a review of the main methods that are taken as a reference for assessing the effect of an albedo surface change in terms of CO<sub>2</sub> compensation is reported. In this context, a correct definition of "surface albedo" is required to avoid confusion and distinguish surface albedo from other contributions. In Figure 1, the main albedo variables associated with the surface, top of atmosphere (TOA), atmosphere, and cloud layers are reported [8].

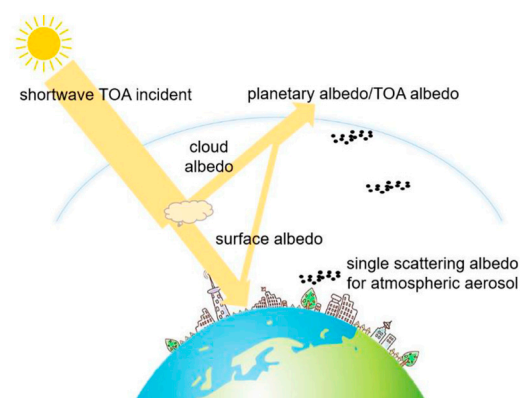


**Figure 1.** The scenario for several essential albedo variables.

In the field of remote sensing, a recent rigorous definition of surface albedo is provided by [8]: "Surface shortwave broadband albedo represents the surface hemispheric reflectivity integrated over the solar spectrum (0.2–5 μm)". In the following discussion, only surface albedo will be taken into account.

Management of Earth's surface albedo is recognized by many authors [9–11] as a strategy for climate change mitigation. Several empirical studies have confirmed that a change in albedo leads to a change on anthroposphere temperature [12,13]. The common approach for assessing the effect of an albedo change involves the radiative forcing concept, which will be later reminded; in this way, albedo change can be put in relation to a change on atmospheric greenhouse gas concentration [14].

Literature approaches differ from one another by the input data and method used to calculate  $RF$ . Moreover, only average data are taken into account despite the fact that  $RF$  is a time variant quantity.

By IPCC definition, the radiative forcing is “the change in net irradiance at the tropopause AFTER allowing for stratospheric temperatures to readjust to radiative equilibrium”. In the shortwave range, there is no evidence that the stratospheric temperature adjusts to a surface albedo change [12,15,16], thus the instantaneous shortwave flux change at the top of the atmosphere ( $TOA$ ) is typically taken as  $RF_{\Delta\alpha}$ , consistent with Myhre et al. [17].

The change in radiative forcing due to a perturbation to the atmospheric  $CO_2$  concentration  $RF_{CO_2}$  is calculated by the following relation [17,18]:

$$RF_{CO_2} = 5.35 \cdot \ln\left(\frac{C_0 + \Delta C}{C_0}\right), \quad (1)$$

$RF_{CO_2}$  when  $\Delta C$  is 1 ppm and  $C_0$  is the actual atmospheric  $CO_2$  concentration, is known as current *global mean radiative efficiency*, or  $\alpha_{CO_2}$  (in  $W/m^2$  ppm). The  $CO_2$  global mean radiative efficiency with units of  $[W/m^2 \text{ kg}]$  can be obtained from  $\alpha_{CO_2}$  by the following equation:

$$k_{CO_2} = \frac{\alpha_{CO_2} \cdot \varepsilon_{air} \cdot 10^6}{\varepsilon_{CO_2} \cdot M_{atm}}, \quad (2)$$

where  $\varepsilon_{CO_2}$  is the molecular weight of  $CO_2$  (44.01 kg/kmol),  $\varepsilon_{air}$  is the molecular weight of air (28.97 kg/kmol), and  $M_{atm}$  is the mass of the atmosphere ( $5.14 \times 10^{18}$  kg). For a  $CO_2$  background concentration of 389 ppm,  $k_{CO_2}$  is equal to  $1.76 \times 10^{-15} W/m^2 \text{ kg}$  [17].

Over the past 20 years, different approaches have been developed to express  $RF_{\Delta\alpha}$  as  $CO_2$  equivalence. A simplified method relates  $RF_{\Delta\alpha}$  to the  $RF$  following a constant in time change of  $CO_2$  concentration. In such a method, a constant amount of the  $CO_2$  emission (defined airborne fraction  $AF$ ) is instantaneously removed by Earth's ocean and terrestrial  $CO_2$  sinks [19]. This method—known as Emissions Equivalent of Shortwave Forcing ( $EESF$ )—was first introduced by Betts [20] as:

$$EESF = \frac{RF_{\Delta\alpha}}{k_{CO_2} \cdot A_E \cdot AF}, \quad (3)$$

where  $EESF$  is expressed in  $kgCO_{2eq}/m^2$ ,  $A_E$  is Earth's surface area ( $5.1 \times 10^{14} m^2$ ), and  $AF$  is the airborne fraction.  $RF_{\Delta\alpha}$  has been simulated by Betts by means of the radiative transfer scheme of the third Hadley Centre Atmosphere Model (HadAM3) for a 20-year period (annual mean).

Akbari [4] calculated a change in  $RF_{\Delta\alpha}$  (at  $TOA$ ) per 0.01 change in solar reflectance of the surface equal to  $-1.27 W/m^2$ . By applying the  $EESF$  method results that the emitted  $CO_2$  equivalent offset for 0.01 increase in albedo of urban surface is equal to  $-2.55 kg CO_{2eq}/m^2$ . Similar results have been obtained by Menon [7]: a change in radiative forcing (for a 0.01 albedo increase) equal to  $-1.63 W/m^2$  and an emitted  $CO_2$  equivalent offset of  $-3.26 kg CO_{2eq}/m^2$ . By means of an analogous approach, Rossi et al. [5] calculated a  $CO_{2eq}$  equivalency of  $-3.20 kg$  of  $CO_{2eq}$  per  $m^2$  of Earth area for a 0.01 change in albedo.

Recently, a more accurate way to calculate the value of  $RF_{\Delta\alpha}$  has been proposed by Sciusco [21]:

$$RF_{\Delta\alpha}(t) = -\frac{1}{N} \sum_{d=1}^N W_{in} \cdot T_a \cdot \Delta\alpha, \quad (4)$$

where  $RF_{\Delta\alpha}$  is the mean albedo-induced radiative forcing at  $TOA$  over a period  $t$  (growing season),  $N$  is the number of days in the chosen period,  $W_{in}$  is the incoming solar radiation at the surface,  $T_a$  is the upward atmospheric transmittance, and  $\Delta\alpha$  is the change in albedo. While previous studies (e.g., Lenton and Vaughan [22] and Cherubini et al. [23]) used a global annual average value of 0.854 for  $T_a$ , Sciusco calculated  $T_a$  as the ratio of incoming solar radiation at the top of the atmosphere ( $W_{TOA}$ ) to that at the surface ( $W_{in}$ ).

In 2016, an alternate time-dependent metric has been proposed by Bright et al. [24] to take into account the time dependency of  $CO_2$  removal processes. This metric is termed Time-Dependent Emissions Equivalence, or  $TDEE$ :

$$TDEE = \frac{RF_{\Delta\alpha}(t)}{k_{CO_2} \cdot A_E \cdot y_{CO_2}(t)}, \quad (5)$$

In Equation (5), the term  $AF$  is replaced by  $y_{CO_2}(t)$ . This function represents the time decay of atmospheric  $CO_2$  concentration after a single pulse emission, and it depends on the interactions between the atmosphere and the oceans and the terrestrial biosphere (Joos, 1996 [25]; Joos et al., 2001 [26]). The analytical form is given by [19]:

$$y_{CO_2}(t) = A_0 + \sum_{i=1}^3 A_i \cdot e^{-t/\beta_i}, \quad (6)$$

where  $A_0 = 0.217$ ,  $A_1 = 0.259$ ,  $A_2 = 0.338$ ,  $A_3 = 0.186$ ,  $\beta_1 = 172.9$ ,  $\beta_2 = 18.51$ , and  $\beta_3 = 1.186$ .

An example of trend plot of  $y_{CO_2}(t)$  is reported in Figure 2. The trend represents the return flux of carbon into the atmosphere after an initial pulse of carbon assimilation at time  $t = 0$ .

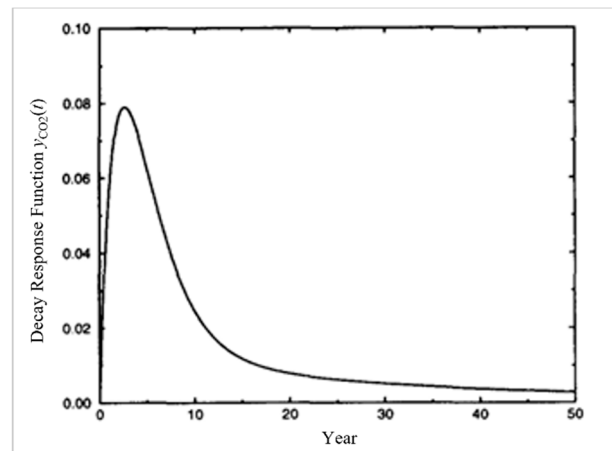


Figure 2. Example of decay response function  $y_{CO_2}(t)$  [25].

The annual ( $t$ ) mean  $RF_{\Delta\alpha}$  is given by:

$$RF_{\Delta\alpha}(t) = \left[ \frac{1}{12} \sum_{m=1}^{12} R_{SW}^{\downarrow}(m) \cdot \Delta\alpha(t, m) \cdot T_{SW}^{\uparrow}(m) \right] \cdot \left( \frac{A}{A_E} \right), \quad (7)$$

where  $R_{SW}$  is the monthly ( $m$ ) mean solar radiation incident on a topographically corrected tilted surface,  $\Delta\alpha$  is the albedo change in month  $m$  and year  $t$ ,  $A$  is the total surface area over which  $\Delta\alpha$  occurs, and  $T_{SW}$  is the same parameter  $T_a$  of Equation (4).

In 2019, Bright [27] has introduced a simplified model for the calculation of the local annual mean instantaneous  $RF_{\Delta\alpha}$ :

$$RF_{\Delta\alpha}(t) = \left[ \frac{1}{12} \sum_{m=1}^{12} -W_{in,m,t} \cdot \Delta\alpha_{m,t} \cdot \sqrt{T_{a,m,t}} \right], \quad (8)$$

where  $W_{in,m,t}$  is the incoming solar radiation flux incident at surface level in month  $m$  and year  $t$  and  $T_{a,m,t}$  is the monthly mean clearness index (or  $W_{in}/W_{TOA}$ ; unitless) in month  $m$  and year  $t$ .

Similar to  $TDEE$  is the Global Warming Potential ( $GWP$ ) metric ([28,29]). In  $GWP$  definition, the term  $RF_{\Delta\alpha}(t)$  is evaluated over a discretized time horizon ( $TH$ ) and it is then normalized to the radiative forcing following a unit pulse  $CO_2$  emission accumulated over the same  $TH$ :

$$GWP_{\Delta\alpha}(TH) = \frac{\sum_0^{t=TH} RF_{\Delta\alpha}(t)}{k_{CO_2} \cdot A_E \cdot \sum_0^{t=TH} y_{CO_2}(t)}, \quad (9)$$

Additionally, in the more accurate literature models,  $RF_{\Delta\alpha}$  is evaluated at discrete time intervals.  $RF_{\Delta\alpha}$  is indeed a continuous time-dependent quantity which varies by several drivers as well as solar path and atmospheric absorption. Therefore, the proper assessment of  $RF_{\Delta\alpha}$ , and therefore of the  $CO_{2eq}$  offset, cannot be exempted from a continuous measurement of  $RF$ .

In Table 1, a comparison among the values of  $CO_2$  offset obtained by means of the previously discussed metrics is reported.

**Table 1.** Comparison among methods for  $CO_2$  offset calculation.

Methods/Models	Metric	$CO_2$ Offset	$\Delta\alpha$	Notes
Betts et al. (2000) [20]	<i>EESF</i>	0.70 kg C/m <sup>2</sup>	0.01	$AF = 0.5$
Akbari et al. (2009) [4]	<i>EESF</i>	2.55 kg $CO_{2eq}$ /m <sup>2</sup>	0.01	$AF = 0.55$
Menon et al. (2010) [7]	<i>EESF</i>	3.26 kg $CO_{2eq}$ /m <sup>2</sup>	0.01	$AF = 0.55$
Rossi et al. (2013) [5]	<i>EESF</i>	3.20 kg $CO_{2eq}$ /m <sup>2</sup>	0.01	$AF = 0.5$
Sieber et al. (2019) [30]	<i>GWP</i>	69 g $CO_{2eq}$ /m <sup>2</sup> year	0.05	$TH = 100$ year
Bright et al. (2021) [14]	<i>EESF</i>	3.50–6.90 kg $CO_{2eq}$ /m <sup>2</sup>	0.04	$AF = 0.3–0.6$
Bright et al. (2021) [14]	<i>TDEE</i>	3.0 kg $CO_{2eq}$ /m <sup>2</sup>	0.04	$TH = 80$ year

Results obtained from different authors by the metric *EESF* are substantially similar and within a range of 1.3–3.3 kg  $CO_{2eq}$ /m<sup>2</sup> for a  $\Delta\alpha = 0.01$ . *GWP* returns values that depend on the time horizon  $TH$  taken into account. Nevertheless, for a “standard”  $TH$  (100 years), the values of *GWP* (1.4 kg  $CO_{2eq}$ /m<sup>2</sup>) are aligned to that obtained by *EESF*.

### 3. The Novel Method

Surface albedo generally varies by land cover type for natural and artificial surfaces and is also sensitive to various factors besides atmospheric and cloud conditions, such as soil–vegetation, snow, topography, diurnal asymmetry, and spatial resolution. A comprehensive literature review of the variance pattern of surface albedo over typical land types and subsequent effects on climate is reported in [31]. In the present paper, only the effect on local climate produced by the change in albedo of artificial surfaces will be indagated, with limited extension.

A novel methodology to determine the in continuo albedo-induced radiative forcing change ( $RF_{\Delta\alpha}$ ) through ground measurements and satellite calibration is herein proposed. In this way, the discussed limitations of literature methods may be overtaken.

The proposed methodology guarantees more precision, since the continuous ground measurements of the radiative forcing take into account variations in solar, atmospheric, and superficial parameters. Then, ground measurements are made more reliable using discrete calibration by satellite measurements. The effectiveness of the albedo increase in the  $CO_2$  offset depends on the variation over time of the albedo itself, so the continuous monitoring and calibration are necessary steps to ensure the methodology is reliable.

The application of the procedure requires the installation of the proper instrumentation on site and the data collection and management both from ground and satellite measurements.

The proposed procedure has no geographical limitations once the surface is equipped with the proper instrumentation and data from the satellite are collected for that specific site. Finally, it is necessary to highlight that the proposed procedure is applied to homogeneous

surfaces. The application of the method to heterogeneous surfaces will be studied in an ongoing survey, which is involving also albedometer-equipped drone measurements.

### 3.1. Model

According to IPCC taxonomy, *GWP* is the ratio of the time-integrated radiative forcing from the instantaneous release of 1 kg of a gas  $x$  relative to that of 1 kg of a reference gas  $R$  (e.g.,  $\text{CO}_2$ ). *GWP* is calculated through the following equation:

$$GWP_x = \frac{\int_0^T k_x \cdot y_x(t) \cdot dt}{\int_0^T k_R \cdot y_R(t) \cdot dt}, \quad (10)$$

where  $T$  is the time horizon over which the calculation is considered;  $k_x$  is the radiative efficiency of gas  $x$ ; and  $y_x(t)$  is the time-dependent decay in abundance of the substance following an instantaneous release of it at time  $t = 0$ . Radiative efficiency is the increase in radiative forcing for a unit increase in the atmospheric abundance of the substance. This parameter is typically expressed in  $\text{W}/\text{m}^2 \text{ kg}$ . The denominator contains the corresponding quantities for the reference gas (i.e.,  $\text{CO}_2$ ).

As previously discussed, the *GWP* concept may be conveniently extended to evaluate the effect of superficial albedo change in terms of equivalent  $\text{CO}_2$ . If albedo is increased, *GWP* becomes negative and may be considered as a  $\text{CO}_2$  well, so  $\text{CO}_2$  is compensated. By that, in Equation (10), the numerator is substituted by the integral of  $RF_{\Delta\alpha}$  time history (Equation (11)) on an observation period  $T$ .

$$\text{CO}_{2, \text{comp}} = \frac{\int_0^T S \cdot RF_{\Delta\alpha}(t) \cdot dt}{\int_0^T A_E \cdot k_r \cdot y_r(t) \cdot dt}, \quad (11)$$

where  $S$  is the area of the Surface Under Test (*SUT*) and  $RF_{\Delta\alpha}$  is a time-dependent parameter relative to a unit area which depends on several factors: (a) instantaneous solar irradiation; (b) atmospheric absorption on downward beams; (c) surface albedo change; and (d) atmospheric absorption on upward beams. Thus, in order to calculate the compensated  $\text{CO}_2$  amount with Equation (11),  $RF_{\Delta\alpha}$  time history must be determined. A continuous satellite measurement of outward radiation from the albedo-changed surface would be required.

However, an alternative method is here proposed which does not require continuous satellite monitoring, since  $RF_{\Delta\alpha}$  time history is conveniently estimated by ground measurements and occasional satellite data are anyway taken into account to calibrate ground measurements.

As shown in Figure 3, to determine the  $RF$  of a given surface, the following parameters are considered:

- $W_{TOA}$ , solar irradiation per unit area at the top of atmosphere which strikes a virtual surface parallel to the *SUT*;
- $W_{in}$ , solar irradiation per unit area which hits the *SUT*; and
- $W_{out}$ , global solar irradiation reflected by *SUT* which exits from the top of atmosphere. Diffusive reflection is supposed.

The spectral range of these precious quantities will be discussed in a proper Section.  $W_{TOA}$  can be determined by precise astronomical deterministic equations [32],  $W_{in}$  is measured by a pyranometer with proper characteristics (see Section 4), and  $W_{out}$  is calculated as in Equation (13). As previously discussed, the parameter  $T_a$  is the solar energy transmission coefficient due to the atmosphere along the downward path:

$$T_a = \frac{W_{in}}{W_{TOA}}, \quad (12)$$

$T_a$  is an instantaneous parameter which depends on location, solar position, and meteorological conditions.  $\alpha$  is the *SUT* albedo. Also,  $\alpha$  is an instantaneous parameter

which depends on the same factors as  $T_a$ , so the correct expression of  $\alpha$  should be  $\alpha(t)$ . It may be also supposed, very confidently, that reflection occurs according to the diffusive pattern (Lambert's law). Albedo is measured by an albedometer, the characteristics of which are described on Section 4.

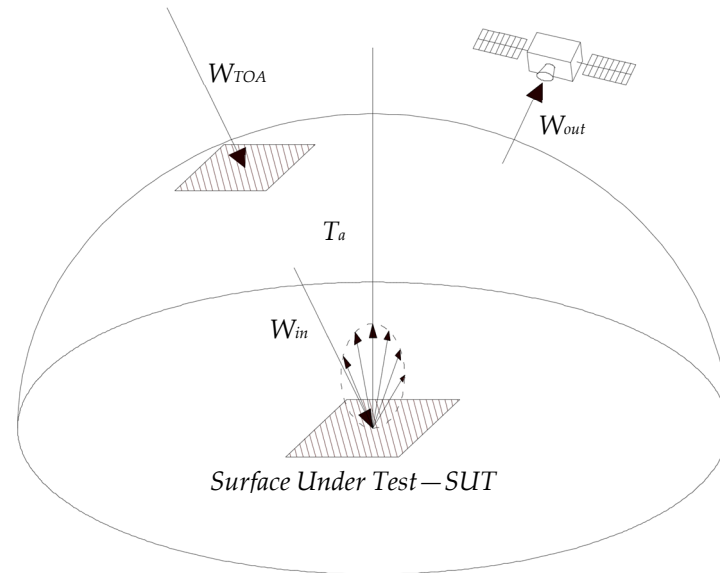


**Figure 3.** Parameters used to determine the  $RF$  of a  $SUT$ .

Assuming that instantaneous atmospheric absorption on the upward path is the same as that of the downward path,  $W_{out}$  may be evaluated as follows:

$$W_{out} = T_a \cdot \alpha \cdot W_{in}, \quad (13)$$

By Equation (12), Equation (13) becomes:

$$W_{out} = \frac{W_{in}^2}{W_{TOA}} \cdot \alpha, \quad (14)$$

$RF$  of  $SUT$  per unit area is defined as:

$$RF = W_{TOA} - W_{out} = W_{TOA} - \frac{W_{in}^2}{W_{TOA}} \cdot \alpha, \quad (15)$$

When  $SUT$  albedo is changed, a change in  $RF$  is also attained, as follows:

$$RF_{\Delta\alpha} = -\frac{W_{in}^2}{W_{TOA}} \cdot \Delta\alpha, \quad (16)$$

Equation (16) can be also rewritten as:

$$RF_{\Delta\alpha} = -W_{in} \cdot T_a \cdot \Delta\alpha, \quad (17)$$

In Equation (15),  $\alpha$  and  $W_{in}$  are continuously measured via proper instrumentation;  $W_{TOA}$  is precisely calculated by astronomical relations [32]. As mentioned before,  $RF_{\Delta\alpha}$  is a time-dependent parameter. Using  $RF_{\Delta\alpha}$  time history in Equation (11), a  $CO_2$  equivalent amount is obtained: when albedo is increased by  $(\alpha_2 - \alpha_1) = \Delta\alpha > 0$ ,  $RF_{\Delta\alpha}$  is also increased, and a negative  $CO_2$  amount comes out, which represents the equivalent compensated  $CO_2$ .

The value of  $RF_{\Delta\alpha}$  depends on several factors, not solely on change in albedo surface; from Equation (17), it can be easily deduced that radiative forcing increases as  $W_{in}$  and  $T_a$

increase. Therefore, the compensation effect of a HAS is greater in regions characterized by high values of incoming radiation and low cloud coverage.

It may be observed that  $RF_{\Delta\alpha}$  comes from a mixed procedure made of measured and calculated quantities, which requires a continuous data acquisition of albedo and ground radiation. Such a mixed procedure is called *RF-meter*, which will be discussed in the next chapter.

### 3.2. Calibration

The proposed methodology to assess  $RF_{\Delta\alpha}$  is accompanied by several errors which may be reduced by a calibration and are discussed hereunder:

- Downward and upward paths generally lay on different directions, which may be characterized by different atmospheric compositions producing different energy absorptions. Furthermore, a more precisely upward path, as shown in Figure 3, is related to a diffusive reflection, which implies a non-unique reflection beam but a spread reflection pattern. Atmospheric layers crossed by upwards paths may obtain different energy absorptions. Atmospheric refraction may also introduce further errors.
- Surface albedo changes during the diurnal time in function of solar zenith angle [33].
- Calculation of  $W_{TOA}$  is affected by intrinsic errors.
- Errors made by albedometer and pyranometer on measuring  $\alpha$  and  $W_{in}$  will be better investigated in Section 4, dedicated to instrumentation.

Affection of errors on  $RF_{\Delta\alpha}$  can be strongly lowered by a calibration procedure carried out by satellite measurements, which can be occasionally carried out on *SUT*. The characteristics of the satellite are discussed in Section 5. As shown in Figure 3, the satellite can sense the *SUT*-reflected energy by which surface albedo is calculated according to a proprietary algorithm (Bonafoni et al. [34]).

Let's call  $\alpha_{sat,i}$  the albedo measured by satellite at the  $i$ -th passage, while  $\alpha_{SUT}(t)$  is the ground continuous measure. It is expected that at the same time of the  $i$ -th satellite passage:

$$\alpha_{sat,i} = \alpha_{SUT}(t_i), \quad (18)$$

However, because of the errors previously discussed, they may differ. Since albedo is required for  $RF_{\Delta\alpha}$  evaluation, at time  $t$ , the most accurate value of *SUT* albedo is the one measured by the satellite (outside the atmosphere). However, albedo satellite measures are available only at discrete times and, in order to evaluate a continuous  $RF_{\Delta\alpha}$ , a continuous *SUT* albedo is required. It is here proposed to use  $\alpha_{sat,i}$  to calibrate the  $\alpha_{SUT}(t)$  according to the following strategy, which introduces a calibration constant  $k_i$  as in Equation (19):

$$k_i = \frac{\alpha_{sat,i}}{\alpha_{SUT}(t_i)}, \quad (19)$$

Thus, on each time interval between  $t_{i+1}$  and  $t_i$ , the calibrated albedo is  $k_i \times \alpha_{SUT}(t)$ . An example of the calibration strategy is reported in Section 6, where preliminary experimental data are shown.

Calibration may be applied also to albedo variation, since errors are not given to ground albedo measurements errors, but rather to atmospheric phenomena, as previously discussed.

Thus, between the  $i$ -th and the  $(i + 1)$ -th satellite passages over the *SUT*, a better estimation of  $RF_{\Delta\alpha}$  is attained by the following relation:

$$RF_{\Delta\alpha,i} = k_i \cdot W_{in} \cdot T_a \cdot \Delta\alpha, \quad (20)$$

$RF_{\Delta\alpha,i}$  is related to the time between the  $i$ -th and the  $(i + 1)$ -th satellite passages.  $RF_{\Delta\alpha,i}$  is a continuous time-dependent quantity calibrated with data coming from the  $i$ -th passage of the satellite.

The evaluation of the calibration constant  $k_i$  can be performed on large scale surfaces, using more than one ground albedo sensor. The number of instruments is chosen in accordance with the satellite spatial resolution (one albedometer for each unit area of the satellite image).

In order to evaluate  $\text{CO}_{2,comp}$  due to *SUT*, the following calibrated equation (Equation (21)) must be calculated instead of Equation (11):

$$\text{CO}_{2,comp} = \frac{\sum_{i=1}^N \int_{T_i}^{T_{i+1}} S \cdot \text{RF}_{\Delta\alpha,i}(t) \cdot dt}{\int_0^T A_E \cdot k_r \cdot y_r(t) \cdot dt}, \quad (21)$$

where  $T_i$  and  $T_{i+1}$  are time values at the  $i$ -th and  $(i + 1)$ -th passages of satellite.  $N$  are the numbers of satellite passages during  $T$ . Obviously, the greater the  $N$ , the more accurate the estimation of  $\text{CO}_{2,comp}$  produced by *SUT*.

#### 4. Experimental Set-Up: RF-Meter

Although several conservative assumptions have been adopted to formulate the proposed procedure, an accurate analysis of errors is required. It will take into account ground measurement errors due mainly to instrumentation, calculation errors due to astronomical equations, and calibration errors.

Further errors will come from operative conditions as well as differential spectral energy absorption along downward and upward paths.

A test facility is here designed to better estimate all the above-mentioned errors and to check the reliability of the proposed procedure (*RF-meter*). Specifically, *RF-meter* will be tested on a properly designed high-albedo surface (*SUT*). Since *RF-meter* procedure is calibrated by remote sensing measurements, satellite characteristics will be chosen as follows:

- minimum spatial resolution: 100 m<sup>2</sup>;
- average revisit time: 5 days;
- spectral characteristics suitable to IPCC radiative forcing definition and albedometer spectral standards.

For reliable satellite sensing, *SUT* is designed to be 900 m<sup>2</sup>; *SUT* is treated by high-reflective paint. *SUT* is located on a flat building roof at the Engineering Department of University of Perugia (43°7'9.449" N, 12°21'27.451" E). *SUT* is equipped with the following instrumentation:

- albedometer, technical features are reported in Table 2;
- weather station;
- Calculus Unit based on Field Point system.

**Table 2.** Technical features of the albedometer LP PYRA 05.

Albedometer <sup>1</sup>	
Technical Features	Specifications
Model	LP PYRA 05
Sensor	Thermopile
Typical sensitivity	10 W/m <sup>2</sup>
Measuring range	0 ÷ 2000 W/m <sup>2</sup>
Viewing angle	2π sr
Spectral range (50%)	305 nm ÷ 2800 nm
Operating temperature	−40 °C ÷ 80 °C

<sup>1</sup> Technical features are referred to the pyranometers, which make up the albedometer LP PYRA 05.

Albedo and incoming irradiation will be measured in accordance with standard ASTM-E1918-06 [35]. Measured data will be processed by a Calculus Unit in order to compute *RF*

time-history and the compensated  $\text{CO}_2$  over a T horizon. Albedometer will be positioned on the *SUT* orthocenter.

An aerial view of the *SUT* is shown in Figure 4.

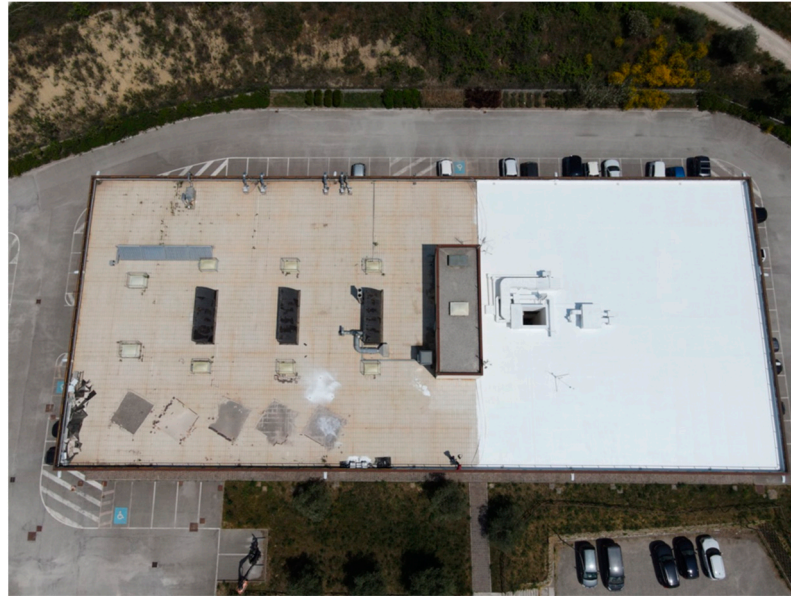


**Figure 4.** An aerial view of the *SUT*.

#### *Spectral Discussion*

Evaluations made in Section 3 have been worked out regardless of the solar energy spectrum. However, spectrum may strongly affect energy balance and  $RF$  estimation.

The IPCC definition for  $RF$  is related to shortwave and longwave radiation [16]; thus, global warming  $\text{CO}_2$  driven phenomena are meant to be correctly described, taking into account the mentioned range.

An albedometer and a pyranometer were used to measure albedo and incoming ground energy, respectively, and are characterized by a 300–2800 nm flat spectral response, while  $W_{TOA}$  represents the calculated extra-atmospheric energy characterized by the entire solar spectrum. Thus, calculation of  $T_a$  in Equation (12) underestimates the instantaneous transmissibility of Earth's atmosphere. Therefore,  $RF_{\Delta\alpha}$  calculated according to Equation (17) is underestimated with respect to the real value. As a consequence,  $\text{CO}_{2,comp}$  is also underestimated. Thus, any possible valorization of  $\text{CO}_{2,comp}$ , as well as the attribution of emission credits, will occur according to a conservative approach.

#### **5. Satellite Characteristics**

Satellite sensors represent an efficient tool for producing surface albedo maps and for monitoring albedo variations with different spatial and temporal resolutions [36]. Furthermore, spectral observations of the solar irradiation reflected by the Earth's surfaces and exiting from the atmosphere can be provided by satellite remote sensing, since the Top-Of-Atmosphere ( $TOA$ ) spectral radiance [ $\text{W}/\text{m}^2 \text{sr mm}$ ] at the sensor aperture is the primary measurement recorded by spaceborne sensors. The total radiation at the sensor consists of two main components: (1) solar radiation scattered by the atmosphere into the sensor's field-of-view and (2) direct and diffuse solar radiation incident on a certain pixel, reflected from the surface, and then transmitted to the sensor.

In choosing an optimal satellite mission for the work purpose, the following requirements must be considered: good spatial resolution, high revisit time, and satellite products in the solar spectrum made available systematically and free of charge to all data users.

Sentinel-2, a multispectral imaging mission within the Copernicus program [37], jointly realized by the EC (European Commission) and ESA (European Space Agency) for global

land observation, fulfills these requirements. The mission comprises a constellation of two identical polar-orbiting satellites (Sentinel-2A and Sentinel-2B) placed in the same sun-synchronous orbit at a mean altitude of 786 km, phased at  $180^\circ$  to each other, with a wide swath width (290 km) allowing a high revisit time (2–3 days at mid-latitudes). Sentinel-2A was launched on 23 June 2015, Sentinel-2B on 7 March 2017. A multi-spectral instrument (MSI) onboard both Sentinel-2 platforms measures the Earth's reflected radiance in 13 spectral bands in the visible (VIS), near-infrared (NIR), and shortwave infrared (SWIR) spectral range, at different spatial resolutions ranging from 10 to 60 m on the ground [38].

The acquisition, processing, archiving, and dissemination of the Sentinel-2 observations at different levels are made available to users via the Copernicus Open Access Hub [39]. From Level-1C product, *TOA* spectral radiances and *TOA* reflectance are achievable, whereas Level-2A product provides at-surface reflectance. Level-1C and Level-2A processing includes radiometric and geometric corrections and orthorectification and spatial registration. Surface reflectance product is obtained by applying an atmospheric correction to *TOA* reflectance product, described in [38].

Several works dealing with the surface albedo estimation from satellite observations were published [40–43]; among different algorithms, narrow-to-broadband conversion methods were developed using surface reflectivity measurements from multispectral satellite sensors [36]. Broadband albedo refers to the albedo computed in the whole solar spectrum, whilst narrowband albedo is computed over a narrow range of wavelengths, i.e., over a single channel of a multispectral sensor. The broadband albedo retrieval from Sentinel-2 was developed and tested in [34] using the surface reflectivities (narrowband albedo) from the VIS-NIR channels at the best spatial resolution (10 m) and from the two window SWIR channels, with native 20 m pixel size, resolved at 10 m with a resolution enhancement method. The 10-m broadband albedo from Sentinel-2 was assessed with ground-based measurements in two different environments (rural and urban), proving to be reliable and accurate (order of 0.02).

## 6. Example of Calibration

In this Section, an example of calibration is reported, based on ground and satellite data acquired on 19 July 2022. The albedo map from Sentinel-2 over the *SUT* (19 July 2022 h. 11:55 local time) is shown in Figure 5. The *SUT* is defined by the white lines, together with the albedometer's position.

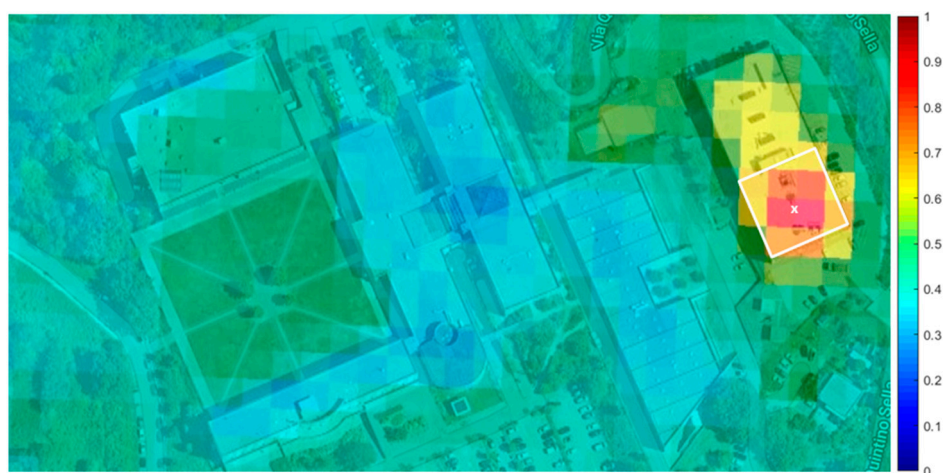


**Figure 5.** Albedo map of the *SUT* from Sentinel-2 satellite—19 July 2022.

The albedo value from Sentinel-2 in the unit area where the albedometer is located is equal to 0.837. At the same time of the satellite passage, the albedo ground measurement is 0.846. Figure 6 shows the ground albedo measurement (blue line) and calibrated albedo (red line).

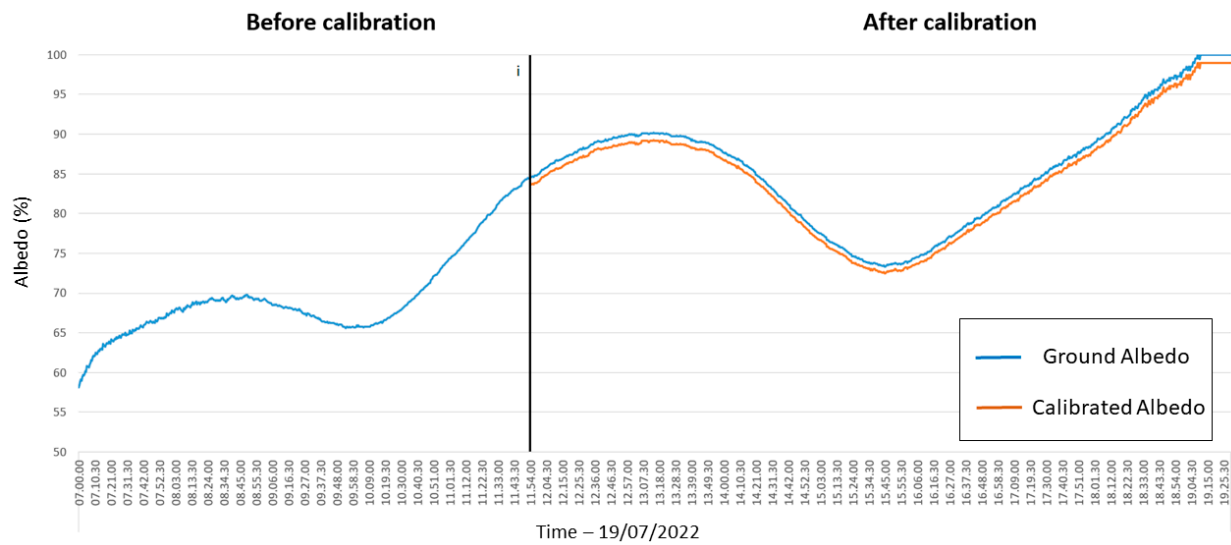


**Figure 6.** Ground albedo measurement (blue line) and calibrated albedo (orange line).

At this point, it is possible to calculate the calibration constant  $k_i$  as in Equation (22):

$$k_i = \frac{\alpha_{sat,i}}{\alpha_{SUT}(t_i)} = \frac{0.837}{0.846} = 0.989 \quad (22)$$

Thus, in the time interval after calibration and before the next satellite passage, the albedo used for  $RF_{\Delta\alpha}$  evaluation is  $0.989 \times \alpha_{SUT}(t)$  as sketched by the red line in Figure 6.

## 7. Conclusions

Emission credits are one of the most effective systems to reduce carbon emissions in the atmosphere and tackle climatic change.

In the European emission market, 1 equivalent ton of  $CO_2$  value is around 100 €, which is predicted to rise due to many factors, such as IPCC climatic change predictions, energy price, and rising social awareness on global warming [44].

Traditional methods to obtain Emission Credits (renewables, CCS, and energy efficiency) are often hard to be implemented and sometimes are uneconomical, at least on a short-term scenario [45].

An alternative but effective method to contrast global warming is the adoption of HAS (high-albedo solution), since they produce an increase of radiative forcing, as the IPCC itself states [1].

Many authors have proposed HAS as a method to obtain emission credits.

However, the quantifications of the amount of  $CO_2$  compensated by HAS are attained by formulas, predictions, or assumptions based on averaged values (see literature paragraph).

This paper proposes a new methodology for assessing the effect of HAS with respect to  $CO_2$  compensation based on a radiative forcing parameter, which is here measured by a particular procedure, the scheme of which is represented in Figure 7. The proposed procedure is called *RF-meter* since it measures *RF* time history and calculates the related  $CO_2$  offset. Satellite observations are also taken into account to periodically calibrate ground measurements.

Equation (21) is the relation which rules *RF-meter*. The proposed methodology is based on conservative assumptions; thus, the calculus of compensated  $CO_2$  (attained by measures) is less than the true value.

Furthermore, an experimental facility is here designed in order to test the proposed methodology and to compare it with literature models. Preliminary results are also reported in order to show and test the calibration procedure.

A discussion is worth conducting about time horizon  $T$ , during which the compensated effect occurs.

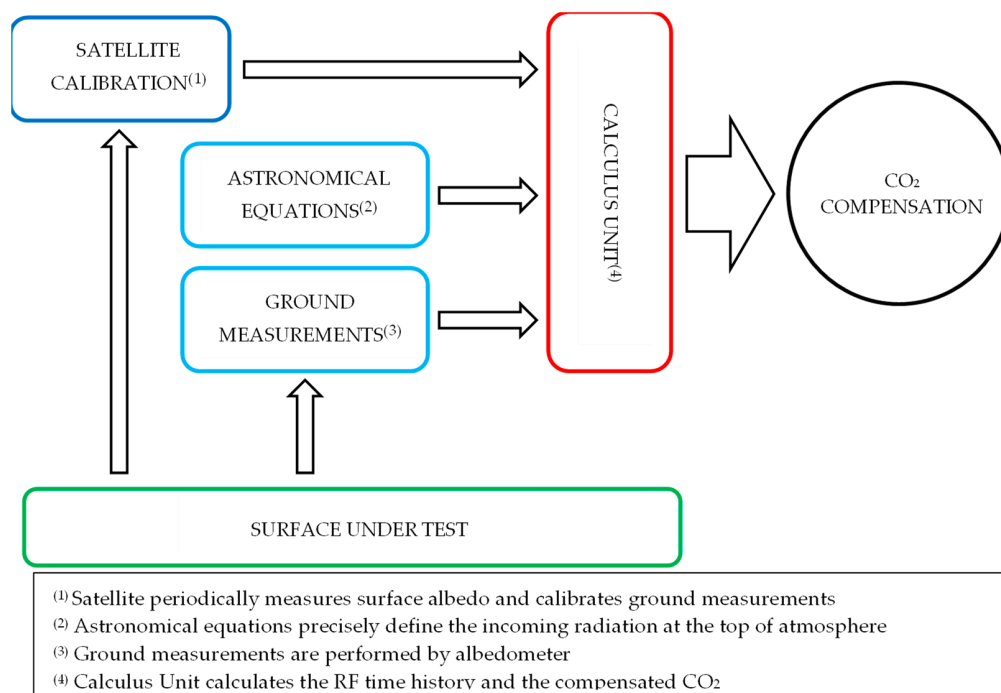


**Figure 7.** RF-meter synoptic scheme.

From Equation (21), it may be observed that the compensation effect of a constant albedo surface (albedo may be eventually preserved by maintenance and cleaning) increases as  $T$  increases because the parameter  $y_r$  (see Equation (11)) decreases; thus, a correct choice of  $T$  is up to emission credits authorities, since economical and strategical consideration must be taken into account. So far, it may be proposed  $T = 1$  year in order to harmonize the HAS compensation effect to emission credits' verification time interval.

The proposed method constitutes, for policy makers and emission credits authorities, an objective and precise tool to assign credits to HAS.

We do believe that such a complementary strategy may be strongly contributory to reinforce the emission credit system on an energy transition period.

**Author Contributions:** Conceptualization, F.R.; methodology, F.R. and B.C.; software, S.B.; validation, F.R.; formal analysis, M.F.; investigation, M.F. and B.C.; resources, M.F.; data curation, M.F.; writing—original draft preparation, F.R. and M.F.; writing—review and editing, B.C., S.B. and C.G.; visualization, M.F.; supervision, F.R.; project administration, F.R. All authors have read and agreed to the published version of the manuscript.

**Funding:** This research received no external funding.

**Institutional Review Board Statement:** Not applicable.

**Informed Consent Statement:** Not applicable.

**Data Availability Statement:** Not applicable.

**Acknowledgments:** The authors acknowledge Watergy International for innovative high albedo materials supply and set up support.

**Conflicts of Interest:** The authors declare no conflict of interest.

## References

1. Edenhofer, O.; Pichs-Madruga, R.; Sokona, Y.; Farahani, E.; Kadner, S.; Seyboth, K.; Adler, A.; Baum, I.; Brunner, S.; Eickemeier, P.; et al. (Eds.) Contribution of Working Group III to the Fifth Assessment Report of the Intergovernmental Panel on Climate Change. In *Climate Change 2014: Mitigation of Climate Change*; Cambridge University Press: Cambridge, UK; New York, NY, USA, 2014.
2. Directive 2003/87/EC; Establishing a System for Greenhouse Gas Emission Allowance Trading within the Union and Amending Council Directive 96/61/EC. European Parliament and of the Council: Washington, DC, USA, 2013.
3. Masson-Delmotte, V.; Zhai, P.; Pirani, A.; Connors, S.L.; Péan, C.; Berger, S.; Caud, N.; Chen, Y.; Goldfarb, L.; Gomis, M.I.; et al. (Eds.) IPCC 2021: Summary for Policymakers. In *Climate Change 2021: The Physical Science Basis. Contribution of Working Group I to the Sixth Assessment Report of the Intergovernmental Panel on Climate Change*; Cambridge University Press: Cambridge, UK; New York, NY, USA, 2021.
4. Akbari, H.; Menon, S.; Rosenfeld, A. Global cooling: Increasing world-wide urban albedos to offset CO<sub>2</sub>. *Clim. Chang.* **2009**, *94*, 275–286. [[CrossRef](#)]
5. Rossi, F.; Cotana, F.; Filippini, M.; Nicolini, A.; Menon, S.; Rosenfeld, A. Cool roofs as a strategy to tackle Global Warming: Economical and technical opportunities. *Adv. Build. Energy Res.* **2013**, *7*, 254–268. [[CrossRef](#)]
6. Taha, H. Urban climates and heat islands: Albedo, evapotranspiration, and anthropogenic heat. *Energy Build.* **1997**, *25*, 99–103. [[CrossRef](#)]
7. Menon, S.; Akbari, H.; Mahanama, S.; Sednev, I.; Levinson, R.M. Radiative forcing and temperature response to changes in urban albedos and associated CO<sub>2</sub> offsets. *Environ. Res. Lett.* **2010**, *5*, 014005. [[CrossRef](#)]
8. Liang, S.; Wang, D.; He, T.; Yu, Y. Remote Sensing of Earth's Energy Budget: Synthesis and Review. *Int. J. Digit. Earth* **2019**, *12*, 737–780. [[CrossRef](#)]
9. Seneviratne, S.I.; Phipps, S.J.; Pitman, A.J.; Hirsch, A.L.; Davin, E.L.; Donat, M.G.; Hirschi, M.; Lenton, A.; Wilhelm, M.; Kravitz, B. Land radiative management as contributor to regional-scale climate adaptation and mitigation. *Nat. Geosci.* **2018**, *11*, 88–96. [[CrossRef](#)]
10. Field, L.; Ivanova, D.; Bhattacharyya, S.; Mlaker, V.; Sholtz, A.; Decca, R.; Manzara, A.; Johnson, D.; Christodoulou, E.; Walter, P.; et al. Increasing arctic sea ice albedo using localized reversible geoengineering. *Earths Future* **2018**, *6*, 882–901. [[CrossRef](#)]
11. Kravitz, B.; Rasch, P.J.; Wang, H.; Robock, A.; Gabriel, C.; Boucher, O.; Cole, J.N.S.; Haywood, J.; Ji, D.; Jones, A.; et al. The climate effects of increasing ocean albedo: An idealized representation of solar geoengineering. *Atmos. Chem. Phys.* **2018**, *18*, 13097–13113. [[CrossRef](#)]
12. Huang, H.; Xue, Y.; Chilukoti, N.; Liu, Y.; Chen, G.; Diallo, I. Assessing global and regional effects of reconstructed land use and land cover change on climate since 1950 using a coupled land–atmosphere–ocean model. *J. Clim.* **2020**, *33*, 8997–9013. [[CrossRef](#)]
13. Laguë, M.M.; Bonan, G.B.; Swann, A.L.S. Separating the impact of individual land surface properties on the terrestrial surface energy budget in both the coupled and uncoupled land–atmosphere system. *J. Clim.* **2019**, *32*, 5725–5744. [[CrossRef](#)]
14. Bright, R.M.; Lund, M.T. CO<sub>2</sub>-equivalence metrics for surface albedo change based on the radiative forcing concept: A critical review. *Atmos. Chem. Phys.* **2021**, *21*, 9887–9907. [[CrossRef](#)]
15. Smith, C.J.; Kramer, R.J.; Myhre, G.; Alterskjær, K.; Collins, W.; Sima, A.; Boucher, O.; Dufresne, J.L.; Nabat, P.; Michou, M.; et al. Effective radiative forcing and adjustments in CMIP6 models. *Atmos. Chem. Phys.* **2020**, *20*, 9591–9618. [[CrossRef](#)]
16. Hansen, J.; Sato, M.; Ruedy, R.; Nazarenko, L.; Lacis, A.; Schmidt, G.A.; Russell, G.; Aleinov, I.; Bauer, M.; Bauer, S.; et al. Efficacy of climate forcings. *J. Geophys. Res. Atmos.* **2005**, *110*, D18104. [[CrossRef](#)]
17. Myhre, G.; Shindell, D.; Bréon, F.; Collins, W.; Fuglestad, J.; Huang, J.; Koch, D.; Lamarque, J.; Lee, D.; Mendoza, B.; et al. Chapter 8: Anthropogenic and Natural Radiative Forcing. In *Climate Change 2013: The Physical Science Basis. Contribution of Working Group I to the Fifth Assessment Report of the Intergovernmental Panel on Climate Change*; Cambridge University Press: Cambridge, UK; New York, NY, USA, 2013; pp. 659–740.
18. Myhre, G.; Highwood, E.J.; Shine, K.P.; Stordal, F. New estimates of radiative forcing due to well mixed greenhouse gases. *Geophys. Res. Lett.* **1998**, *25*, 2715–2718. [[CrossRef](#)]
19. Forster, P.; Ramaswamy, V.; Artaxo, P.; Bernsten, T.; Betts, R.; Fahey, D.W.; Haywood, J.; Lean, J.; Lowe, D.C.; Myhre, G.; et al. Changes in atmospheric constituents and in radiative forcing. In *Climate Change 2007: The Physical Science Basis. Contribution of Working Group I to the Fourth Assessment Report of the Intergovernmental Panel on Climate Change*; Cambridge University Press: Cambridge, UK; New York, NY, USA, 2007.
20. Betts, R.A. Offset of the potential carbon sink from boreal forestation by decreases in surface albedo. *Nature* **2000**, *408*, 187–190. [[CrossRef](#)]
21. Sciusco, P.; Chen, J.; Abraha, M.; Lei, C.; Robertson, G.P.; Laforteza, R.; Shirkey, G.; Ouyang, Z.; Zhang, R.; John, R. Spatiotemporal variations of albedo in managed agricultural landscapes: Inferences to global warming impacts (GWI). *Landsc. Ecol.* **2020**, *35*, 1385–1402. [[CrossRef](#)]
22. Lenton, T.M.; Vaughan, N.E. The radiative forcing potential of different climate geoengineering options. *Atmos. Chem. Phys.* **2009**, *9*, 5539–5561. [[CrossRef](#)]
23. Cherubini, F.; Bright, R.M.; Strømman, A.H. Site-specific global warming potentials of biogenic CO<sub>2</sub> for bioenergy: Contributions from carbon fluxes and albedo dynamics. *Environ. Res. Lett.* **2012**, *7*, 045902. [[CrossRef](#)]

24. Bright, R.M.; Bogren, W.; Bernier, P.Y.; Astrup, R. Carbon equivalent metrics for albedo changes in land management contexts: Relevance of the time dimension. *Ecol. Appl.* **2016**, *26*, 1868–1880. [[CrossRef](#)]
25. Joos, F.; Bruna, M. Pulse response functions are cost-efficient tools to model the link between carbon emissions, atmospheric CO<sub>2</sub> and global warming. *Phys. Chem. Earth* **1996**, *21*, 471–476. [[CrossRef](#)]
26. Joos, F.; Prentice, I.C.; Sitch, S.; Meyer, R.; Hooss, G.; Plattner, G.K.; Gerber, S.; Hasselmann, K. Global warming feedbacks on terrestrial carbon uptake under the Intergovernmental Panel on Climate Change (IPCC) emission scenarios. *Glob. Biogeochem. Cycles* **2001**, *15*, 891–907. [[CrossRef](#)]
27. Bright, R.M.; O'Halloran, T.L. Developing a monthly radiative kernel for surface albedo change from satellite climatologies of Earth's shortwave radiation budget: CACK v1.0. *Geosci. Model Dev.* **2019**, *12*, 3975–3990. [[CrossRef](#)]
28. Shine, K.; Derwent, R.G.; Wuebbles, D.J.; Morcrette, J.J. Radiative forcing of climate. In *Climate Change: The IPCC Scientific Assessment*; Cambridge University Press: New York, NY, USA; Melbourne, Australia, 1990.
29. Rogers, J.D.; Stephens, R.D. Absolute infrared intensities for F-113 and F-114 and an assessment of their greenhouse warming potential relative to other chlorofluorocarbons. *J. Geophys. Res. Atmos.* **1988**, *93*, 2423–2428. [[CrossRef](#)]
30. Sieber, P.; Ericsson, N.; Hansson, P.A. Climate impact of surface albedo change in Life Cycle Assessment: Implications of site and time dependence. *Environ. Impact Assess. Rev.* **2019**, *77*, 191–200. [[CrossRef](#)]
31. Zhang, X.; Jiao, Z.; Zhao, C.; Qu, Y.; Liu, Q.; Zhang, H.; Tong, Y.; Wang, C.; Li, S.; Guo, J.; et al. Review of Land Surface Albedo: Variance Characteristics, Climate Effect and Management Strategy. *Remote Sens.* **2022**, *14*, 1382. [[CrossRef](#)]
32. Iqbal, M. *An Introduction to Solar Radiation*; Academic Press: Cambridge, MA, USA, 1983.
33. Liu, J.C.; Schaaf, C.B.; Strahler, A.H.; Jiao, Z.T.; Shuai, Y.M.; Zhang, Q.L.; Roman, M.O.; Augustine, J.A.; Dutton, E.G. Validation of Moderate Resolution Imaging Spectroradiometer (MODIS) albedo retrieval algorithm: Dependence of albedo on solar zenith angle. *J. Geophys. Res.-Atmos.* **2009**, *114*, D1106. [[CrossRef](#)]
34. Bonafoni, S.; Sekertekin, A. Albedo retrieval from Sentinel-2 by new narrow-to-broadband conversion coefficients. *IEEE Geosci. Remote Sens. Lett.* **2020**, *17*, 1618–1622. [[CrossRef](#)]
35. *ASTM-E1918-06*; Standard Test Method for Measuring Solar Reflectance of Horizontal and Low-Sloped Surfaces in the Field. ASTM International, ASTM: West Conshohocken, PA, USA, 2015; pp. 1–3.
36. Liang, S. Narrowband to broadband conversions of land surface albedo—I Algorithms. *Remote Sens. Environ.* **2001**, *76*, 213–238. [[CrossRef](#)]
37. Copernicus Program. Available online: [http://www.esa.int/Our\\_Activities/Observing\\_the\\_Earth/Copernicus/Overview4](http://www.esa.int/Our_Activities/Observing_the_Earth/Copernicus/Overview4) (accessed on 10 June 2022).
38. Sentinel-2 Missions. Available online: <https://sentinel.esa.int/web/sentinel/user-guides/sentinel-2-msi> (accessed on 10 June 2022).
39. Copernicus Open Access Hub. Available online: <https://scihub.copernicus.eu/dhus/#/home> (accessed on 10 June 2022).
40. Qu, Y.; Liang, S.; Liu, Q.; He, T.; Liu, S.; Li, X. Mapping Surface Broadband Albedo from Satellite Observations: A Review of Literatures on Algorithms and Products. *Remote Sens.* **2015**, *7*, 990–1020. [[CrossRef](#)]
41. Wang, D.; Liang, S.; He, T.; Yu, Y.; Schaaf, C.; Wang, Z. Estimating daily mean land surface albedo from MODIS data. *J. Geophys. Res.-Atmos.* **2015**, *120*, 4825–4841. [[CrossRef](#)]
42. He, T.; Zhang, Y.; Liang, S.; Yu, Y.; Wang, D. Developing land surface directional reflectance and albedo products from geostationary GOES-R and Himawari data: Theoretical basis, operational implementation, and validation. *Remote Sens.* **2019**, *11*, 2655. [[CrossRef](#)]
43. Guo, T.; He, T.; Liang, S.; Roujean, J.; Zhou, Y.; Huang, X. Multi-decadal analysis of high-resolution albedo changes induced by urbanization over contrasted Chinese cities based on Landsat data. *Remote Sens. Environ.* **2022**, *269*, 112832. [[CrossRef](#)]
44. Gasparrini, A.; Guo, Y.; Sera, F.; Vicedo-Cabrera, A.M.; Huber, V.; Tong, S.; Coelho, M.D.S.Z.S.; Saldiva, P.H.N.; Lavigne, E.; Correa, P.M.; et al. Projections of temperature-related excess mortality under climate change scenarios. *Lancet Planet Health* **2017**, *1*, e360–e367. [[CrossRef](#)]
45. Howie, P.; Atakhanova, Z. Assessing initial conditions and ETS outcomes in a fossil-fuel dependent economy. *Energy Strategy Rev.* **2022**, *40*, 100818. [[CrossRef](#)]